ACS APPLIED MATERIALS & INTERFACES

Research Article

Cite This: ACS Appl. Mater. Interfaces 2018, 10, 32597−32606

www.acsami.org

Enhanced Field Modulation Sensitivity and Anomalous Polarity-Dependency Emerged in Spatial-Confined Manganite Strips

Hao Kuang,[†,‡] Jing Wang,*[,†,‡] Jia Li,[†,‡] Kaiming Qiao,[†,‡] Yao Liu,[†,‡] Fengxia Hu,*[,†,‡] Jirong Sun,[†,‡] and Baogen Shen[†,‡]

[†]Beijing National Laboratory for Condensed Matter Physics and State Key Laboratory of Magnetism, Institute of Physics, Chinese Academy of Sciences, Beijing 100190, P. R. China

[‡]School of Physical Sciences, University of Chinese Academy of Sciences, Beijing 100049, P. R. China

S *Supporting Information*

ABSTRACT: An anomalous polarity-dependent electrostatic field modulation effect, facilitated by spatial confinement, is found in an oxide-based field-effect prototype device with a spatial-confined $Pr_{0.7}(Ca_{0.6}Sr_{0.4})_{0.3}MnO_3$ channel. It is revealed that the dominant field modulation mode under a small bias field varies from a polarity-independent strain-mediated one to a nonvolatile polarity-dependent one with enhanced modulation sensitivity as the channel width narrows down to several micrometers. Specially, in the structure confined to length scales similar to that of the phase domains, the field modulation exhibits a greatly increased modulation amplitude around the transition temperature and an anomalous bias-polarity dependence that is diametrically opposite to the normal one observed in regular polarization field-effect. Further simulations show that a large in-plane polarization field is unexpectedly induced by a small out-of-plane bias field of 4 kV/cm in the narrow strip (up to 790 kV/cm for the 3 μm strip). Such large in-plane polarization field, facilitated and enhanced by size reduction, drives phase transitions in the narrow channel film, leading to the reconfiguration of percolation channel and nonvolatile modulation of transport properties. Accordingly, the accompanied polarity relationship between the induced in-plane polarization field and the applied vertical bias field well explains the observed anomalous polarity-dependence of the modulation. Our studies reveal a new acting channel in the nanoscale control of lateral configurations of electronic phase separation and macroscopic behaviors by a small vertical electric bias field in spatial-confined field-effect structures. This distinct acting mechanism offers new possibilities for designing low-power all-oxide-based electronic devices and exploiting new types of multifunctionality to other strongly correlated materials where electronic phase competition exists.

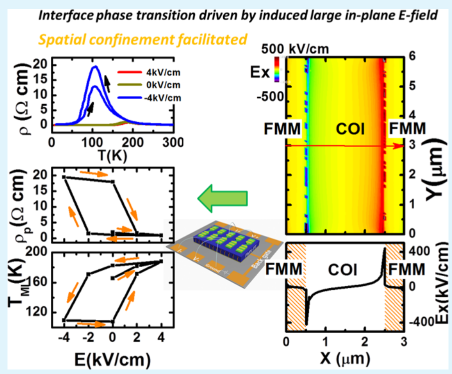

KEYWORDS: *anomalous polarity-dependence, spatial confinement, electrostatic field effect, electronic phase separation, ferromagnetic metal edge state*

I. INTRODUCTION

In the classic electrostatic field-effect configuration, the electrical charge carrier density and hence the electrical resistance of a thin channel are precisely modulated by external electrical voltage, providing electrical switching capability. The application of this remarkably simple but very successful approach expedites the powerful electronic device-semiconducting field-effect transistors (FETs), laying a good foundation of the modern electronics era. Excited by the success of electrostatic field-effect in classic semiconductors, dozens of groups have tried to apply this approach in recent years to the novel correlated electron systems whose properties depend strongly on the carrier concentration. These materials have attracted considerable attention due to the observation of many extraordinary physical phenomena such as high-temperature superconductivity, colossal magnetoresistance, metal−insulator transition (MIT), and multiferrocity. Specially, these novel behaviors are often accompanied by coexisting electronic and magnetic phases, resulting from strong correlations among charge, spin, orbital, and lattice degrees of freedom.[1−5] These energetically degenerate phases coexist and compete with each other, creating a subtle balanced system that can be drastically modified with small changes to the underlying parameters.

Manipulating the balance between electronic and magnetic phases in a correlated electron system, in particular manganite oxides,[6,7] through external field provides new opportunities for fundamental physics research[8−15] and innovative device applications, including novel field-effect switching and non-volatile memory devices.[16−19] Several attempts have been made to achieve nonvolatile electrostatic modulation in field-effect configurations with all-perovskite-structure, where dielectrics/ferroelectrics (FEs) serve as the gate oxide and manganite films

Received: July 3, 2018
Accepted: September 3, 2018
Published: September 3, 2018

DOI: 10.1021/acsami.8b10915
ACS Appl. Mater. Interfaces 2018, 10, 32597−32606

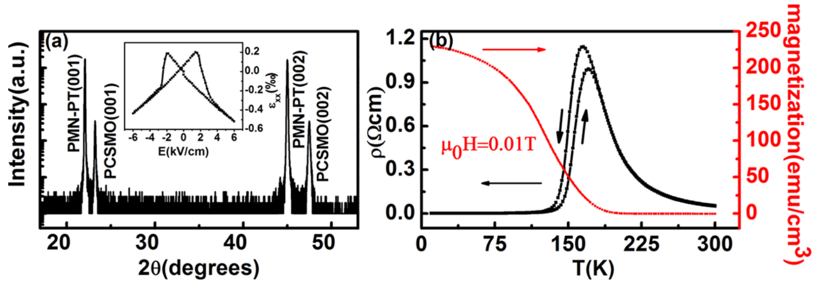

Figure 1. (a) θ−2θ scan patterns of as-prepared 100 nm PCSMO/PMN−PT film. (b) Temperature-dependent magnetization under a magnetic field of 0.01 T and resistance for the as-prepared film before lithographic processing. Inset of (a) shows in-plane strain versus E for the PMN−PT(001) substrate.

as the channel layer.[14,20−23] However, research demonstrated that the electrostatic modulation is strongly entangled with the strain effect,[24−29] resulting from the inverse piezoelectric effect of the ferroelectric (FE) substrate/layer, which is polarity-independent and volatile, which restricts its further investigation and possible potential application. Moreover, most obtained electrostatic field effects, particularly for the high-carrier-density systems such as wide-band manganites, were limited by the short Thomas−Fermi screening length of less than 1 nm, which results in the requirement of an extremely large electric field (or polarization field) to achieve substantial field modulation. These special characteristics make the studies of nonvolatile electrostatic modulation in manganite oxides bog down. Fortunately, recent studies found that the polarized electric field could penetrate deeply into the narrow-band manganite film with phase separation (PS) through an electronically inhomogeneous channel,[20,30] breaking through the limitation of screening effect. However, recent discoveries of the large influence of dimension reduction on the phase separation and thus percolation channel bring new challenges in practice.

Many studies have shown that the length scale of the phase-separated (PS) regions/domains ranges from micrometers to nanometers. Although most experimental studies and prototype device investigations in manganite oxides are based on modulating the macroscopic behaviors by applying global electric field,[6,7,26,31−33] local control of magnetic and electronic properties in spatial-confined systems by means of electrostatic field effect is of special importance for revealing the underlying mechanism and the potential nanodevice application.[34] Recently, spatial confinement at length scales similar to, or even less than, that of the inherent PS domains has been used to induce various quasi-one-dimensional magnetic and electronic behaviors such as intrinsic tunneling,[35] single pathway re-emergent MIT,[36,37] and ferromagnetic metal (FMM) edge state,[38] where the phase transition and accompanied percolative transport are dominated by a relatively few domains[35,39] and very sensitive to multiple types of fields.[35,40,41] Naturally, one may expect that the combination of spatially confined geometries with local electrostatic field modulation can allow one to access emergent field-modulating behaviors substantially different from those in thin-film systems. In addition, the possibility of modulating the electronic properties of spatially confined electronic phase-separated systems composed of a small number of PS domains will allow examining fundamental issues of nanoscale phase separation and establishing new functionalities for potential uses in oxide multifunctional nanodevices.

In this work, we report an anomalous polarity-dependent electrostatic field modulation effect emerged in spatial-confined $Pr_{0.7}(Ca_{0.6}Sr_{0.4})_{0.3}MnO_3$ (PCSMO) strips. It is demonstrated that the dominant mode of field-modulating behaviors under a small bias electric field (4 kV/cm) varies with reducing the strip width, changing from a volatile and polarity-independent strain-mediated field effect to a nonvolatile polarity-dependent effect with enhanced modulation amplitude. Especially, in structures confined to length scales similar to that of the phase domains, the field modulation exhibits a greatly increased modulation amplitude around transition temperature and an anomalous polarity-dependence, where the positive (negative) bias results in an increase (decrease) of both metallicity and metal−insulator transition temperature, diametrically opposite to the normal one observed in regular polarization field-effect. Calculations of the three-dimensional distribution of electric field intensity in manganite strips based on finite-element analysis show that a large in-plane electric field (or polarization field) is induced by a 4 kV/cm bias field, near the interface between ferromagnetic metal (FMM) and charge-ordered insulator (COI) phases in the narrow strip, and rapidly enhanced with the reduction of strip width (reaching ∼790 kV/cm in 3 μm width strip with FMM domains embedded). Such large in-plane polarization field can drive FMM phases to expand or shrink through accumulating different charges (holes or electrons) at the interface between FMM and COI phases, leading to the reconfiguration of percolation channel and nonvolatile modulation of transport properties. The enhanced in-plane polarization field and limited percolation channel in narrower strips greatly increase the modulation sensitivity. Meanwhile, the accompanied polarity relationship between the induced in-plane polarization field and the applied vertical bias results in the observed anomalous polarity-dependence of the modulation. This unique acting channel of the field modulation offers new possibilities for designing low-power all-oxide-based functional devices and exploiting new types of multifunctionality in other strongly correlated materials where electronic phase competition exists.

II. EXPERIMENTAL SECTION

The typical phase-separated manganite PCSMO was chosen as the prototype material to investigate local electrostatic field modulation for its relatively large size of separated phases that are accessible with standard photolithography techniques. In addition, the strong interaction between coexisting COI and FMM phases in PCSMO leads to the local energetic balance between COI and FMM phases near MIT.[42] This subtle balance could be broken by the external field, resulting in the redistribution of two phases and modulation of MIT. Moreover, the significantly different resistive properties of COI and FMM domains provide an effective channel to transfer the polarization field into the film. The (001)-cut perovskite-type single-crystal $0.7Pb(Mg_{1/3}Nb_{2/3})O_3$−$0.3PbTiO_3$ (PMN−PT) with excellent dielectric/ferroelectric behavior, on which a typical butterfly ε−E curve and coercive field of ~2 kV/cm were obtained (inset of Figure 1a), was chosen as the gate oxide to provide a large polarization field so that an all-perovskite field-effect configuration was constructed. A 100 nm-thick $Pr_{0.7}(Ca_{0.6}Sr_{0.4})_{0.3}MnO_3$ (PCSMO) film was grown epitaxially on (001)-oriented PMN−PT substrate using pulsed laser deposition. The crystalline structure of the film was characterized by a high-resolution X-ray diffractometer (Bruker AXS D8 Discover) using Cu Kα radiation. The magnetic and transport properties were measured with the superconducting quantum interference device, equipped with an electric-measurement module.

Figure 1a shows the θ−2θ scan patterns of the as-prepared film, demonstrating a high orientation along the out-of-plane direction without detectable impurity phases. It was determined from the diffraction patterns that the film undergoes a compress strain of −0.62% at c-direction. Figure 1b presents the temperature dependence of the magnetization (0.01 T) and resistance for the as-prepared film before lithographic processing, which exhibits a typical metal−insulator transition at 166 K (cooling process) with a thermal hysteresis about 7 K due to the first-order phase transition nature. The COI and FMM phases coexist near the metal−insulator transition and strongly interact to maintain a local energetic balance.[43−45] With decreasing temperature, the fraction of the metallic phase gradually increases and the percolation transport network is built,[46,47] resulting in the drop of resistance.

The film was further patterned using photolithography to create strips with widths of 50, 20, 10, 5, and 3 μm, ranging from the length scale much larger than the characteristic domain size of PCSMO to the one comparable. Five Au pads were coated onto the surface of each strip to serve as current−voltage and top-gate electrodes separately. A 150 nm-thick Au was coated onto the back of the substrate to serve as the back-gate electrode. Figure 2b shows the schematic diagram of the experimental device configuration where each PCSMO strip is set in a four-probe geometry. The resistance of the strip is measured using a 50 nA constant current. A Keithley 6517 electrometer was used to apply the gate electric field on the substrate of PMN−PT.

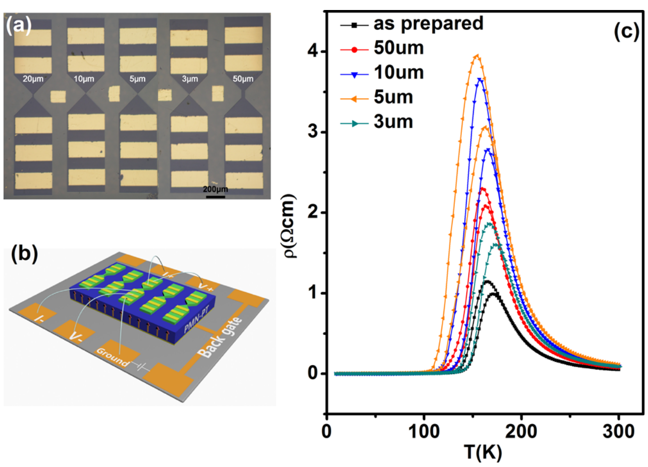

Figure 2. (a) Micrographic image of patterned devices with widths of 3, 5, 10, and 50 μm. (b) Schematic diagram of the experimental device configuration where each PCSMO strip is set in a four-probe geometry. (c) Temperature-dependent resistances of the as-prepared film and patterned strips with varying widths etched from the same 100 nm-thick film in the absence of electric bias voltage.

III. RESULTS AND DISCUSSION

Figure 2c displays the comparison of the temperature-dependent resistance of the parent film and patterned strips without electric voltage on the gate electrode. It was found that the resistance of the strips generally increases in the entire measuring temperature range, accompanied by a gradual decrease of MIT temperature (T_{MI}), when the width reduces toward the individual domain length scale. This behavior of enhanced resistivity and reduced MIT temperature is consistent with previous reports in other mixed-phase manganites[39,41] and should be attributed to the dimensionally limited percolation resulting from the spatially confined conducting channel. Actually, narrower strips have fewer possible percolation paths due to the spatial confinement,[41,48] resulting in the reduction of T_{MI} and increase of resistivity around T_{MI}. Further reducing the width to the level comparable to the domain length scales results in an abnormal decrease in the resistivity and an increase in the temperature of MIT, which might be due to the emergence and enhancement of FMM edge state in the narrow strips. Previous studies have shown that an FMM edge state exists in manganite strips due to the broken symmetry effect, which induces ferromagnetism in the edge region of narrow strips, leading to an increased curie temperature (or MIT temperature) and reduced resistivity.[38]

Figures 3 and 4 show transport behaviors of PCSMO strips with different widths when various electric bias voltages are applied on the gate. In each case, the resistance of the strip is largely modulated by the bias field in the whole temperature range despite the short Thomas−Fermi screening length (~0.2−0.3 nm).[23] This is not surprising since inhomogeneous conducting regions, that is, separated FMM and COI phases, coexist in the PCSMO film near T_{MI}. However, different bias-polarity dependencies are found for the modulation in the strips with different widths. Figure 3c−f shows the variation of the peak resistivity (ρ_p) and metal−insulator transition temperature (T_{MI}) during the cooling process for strips with widths of 50 and 20 μm, respectively, as the bias E-field is cycled from 0 to 4 to −4 kV/cm. One could find that ρ_p (and T_{MI}) decreases (increases) monotonously with the bias E-field regardless of polarity, indicating the polarity independence of the field modulation in both wider strips.

This obvious polarity independence of modulation, in particular near T_{MI}, likely comes from the field-induced strain effect that has been widely observed in manganite−piezoelectric heterostructural films. Many experimental investigations have shown that the electric field applied on the piezoelectric substrate would induce a compressive piezo-strain in the film above and modulate its lattice distortion, resulting in the strain-mediated field modulation of magnetic and transport behaviors through Jahn−Teller coupling.[24−26,31−33,49] Since the piezo-strain is irrelevant to the polarity of E-field (usually exhibits a butterfly shape),[24] the modulation of transport properties originating from the strain effect shows polarity independence. In our strips with large width (>10 μm), the polarity-independent compressive strain induced by E-field (see Figure 3) reduces the epitaxial tensile strain in the PCSMO film, suppressing Jahn−Teller distortion and thus the stability of charge-orbital ordering phases. As a result, the metallicity (or conductivity) and the metal−insulator transition temperature of the strip increase monotonously with the electric field (from 160 to 172 K under 4 kV/cm for the 50 μm strip, and from 175 to 183 K for the 20 μm strip), independent of the bias polarity. Meanwhile, one could also find that the modulation of ρ_p and T_{MI} in wide strips vanishes after the removal of gate voltage, which coincides with the volatility of the field-induced strain effect.[24,25,31,32,49] All these results suggest that, in a wider strip, the strain effect dominates over the E-field-modulating behavior. In addition, the percentage modulation of ρ_p under the field of 4

DOI: 10.1021/acsami.8b10915
ACS Appl. Mater. Interfaces 2018, 10, 32597−32606

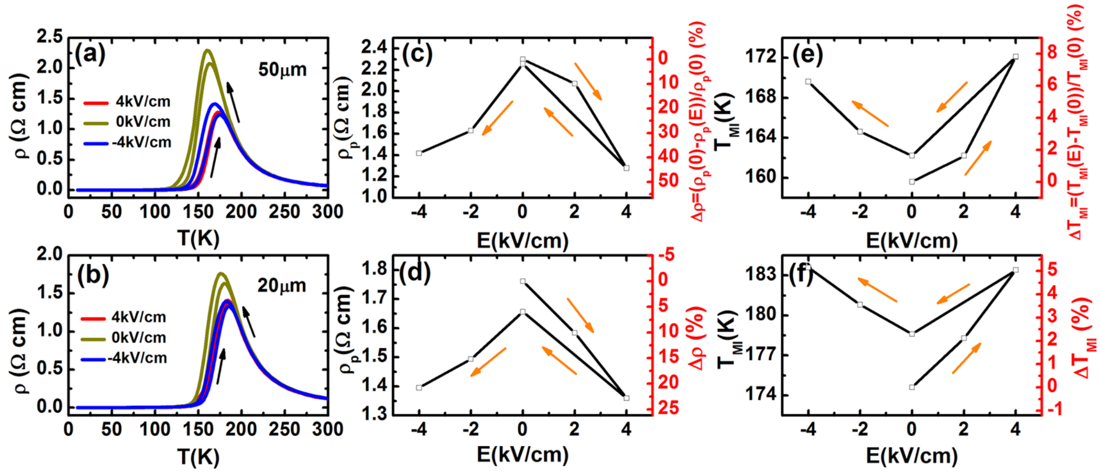

Figure 3. (a, b) Temperature-dependent resistivity under different bipolar electric bias voltages for PCSMO strips with widths of 50 and 20 μm. (c, d) Variation of the peak resistivity ρ_p and (e, f) metal−insulator transition temperature T_{MI} with electric bias field for each strip. The T_{MI} is defined as the temperature of the transition point in the cooling curve, while ρ_p is the resistivity at T_{MI} of the respective strip. Both ρ_p and T_{MI} are determined from the curve in the cooling process. The bias E-field is cycled from 0 to 4 to −4 kV/cm, shown by orange arrows.

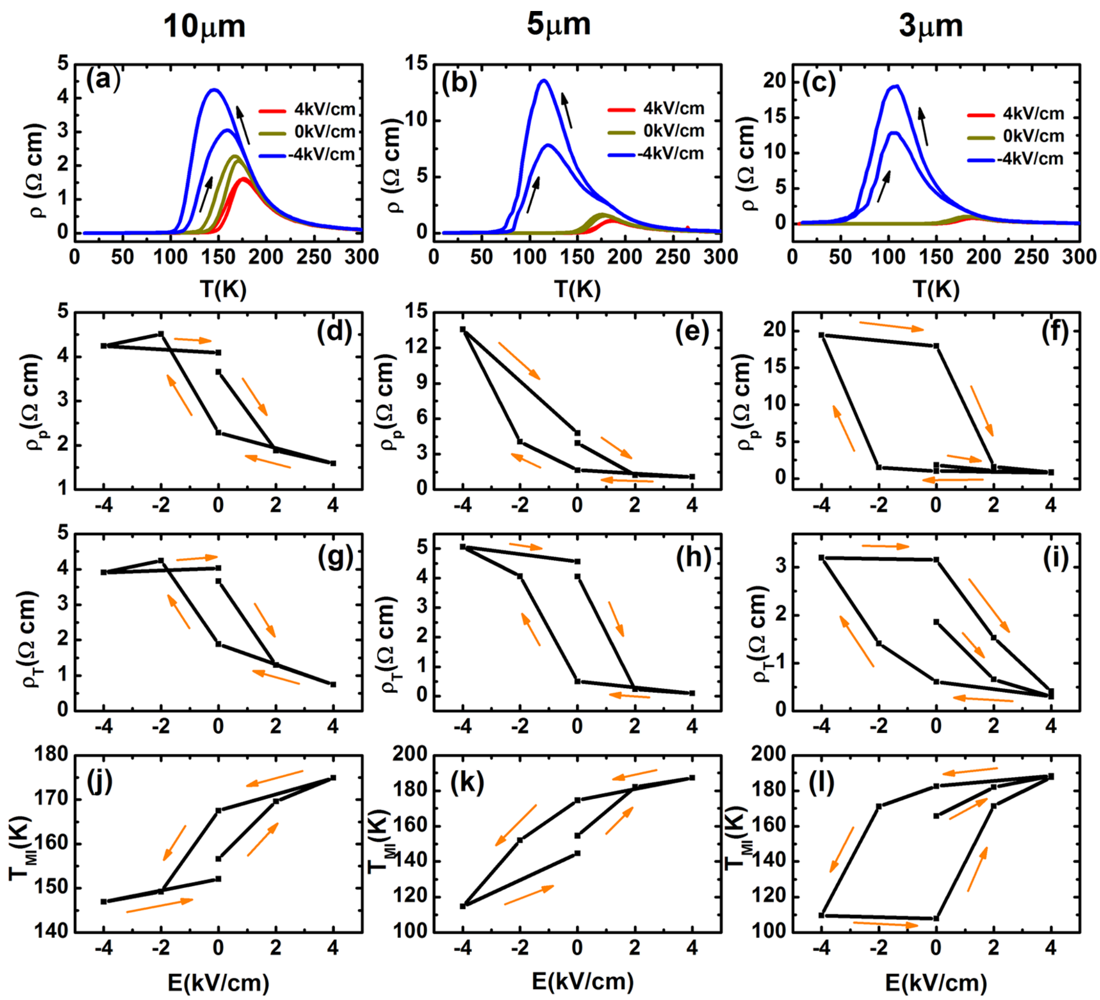

Figure 4. (a−c) Temperature-dependent resistivity under different bipolar electric bias voltages for PCSMO strips with widths of 10, 5, and 3 μm. (d−f) Variation of ρ_p, (g−i) ρ_T, and (j−l) T_{MI} with electric bias field for each strip. The ρ_T is the resistivity at a fixed temperature T_{MI} (0 kV/cm) of the original measured curve for each strip (the black one in (a−c)). All data of ρ_p, ρ_T, and T_{MI} are determined from curves in the cooling process. The bias E-field is cycled from 0 to 4 to −4 to 0 kV/cm, shown by orange arrows. Note that for the 3 μm strip, the field cycling extends to 4 kV/cm due to its FMM edge state in the original stage.

DOI: 10.1021/acsami.8b10915
ACS Appl. Mater. Interfaces 2018, 10, 32597−32606

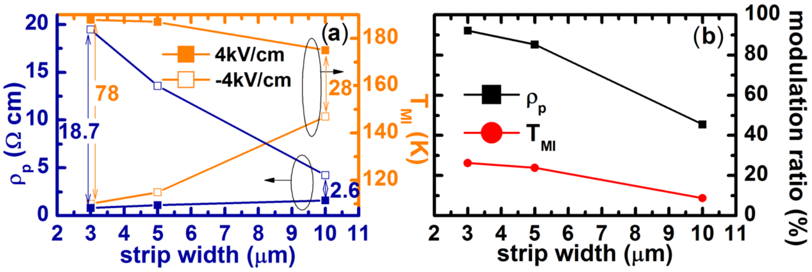

Figure 5. (a) Variation of peak resistivity ρ_p (left axis) and transition temperature T_{MI} (right axis) with the strip width under bias fields of 4 and −4 kV/cm. (b) Modulation ratio of ρ_p and T_{MI} for strips with different widths. The ratios are defined as $|\rho_p(-4\ \mathrm{kV/cm}) - \rho_p(4\ \mathrm{kV/cm})|/(\rho_p(-4\ \mathrm{kV/cm}) + \rho_p(4\ \mathrm{kV/cm}))$ and $|T_{MI}(-4\ \mathrm{kV/cm}) - T_{MI}(4\ \mathrm{kV/cm})|/(T_{MI}(-4\ \mathrm{kV/cm}) + T_{MI}(4\ \mathrm{kV/cm}))$, respectively.

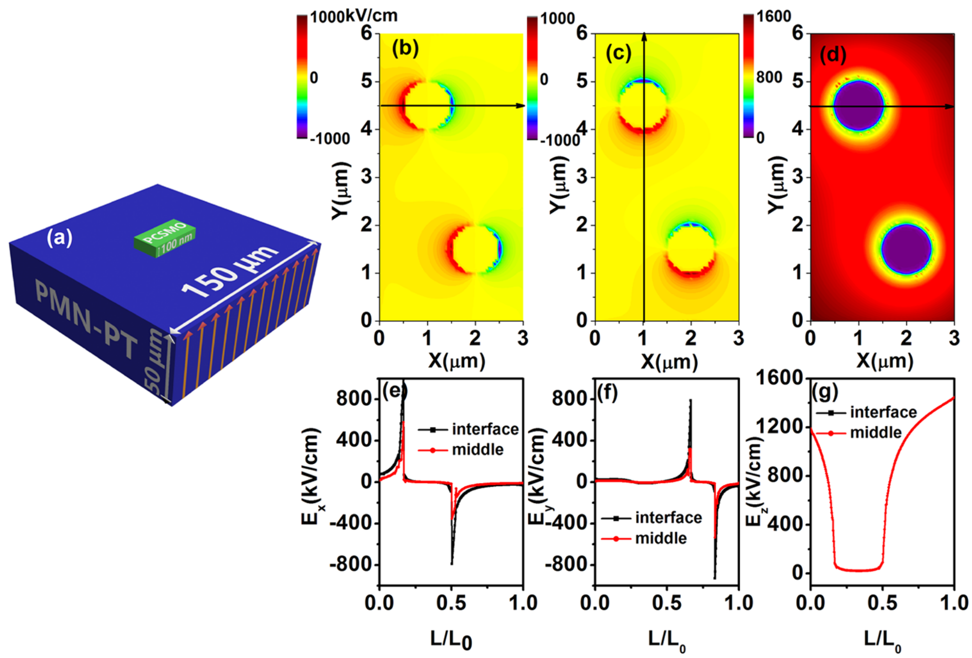

Figure 6. (a) Sketch of the simulating model. (b−d) Two-dimensional distribution of in-plane and out-of-plane *E*-field intensities E_x, E_y, and E_z in the interface plane under +4 kV/cm bias field for the selected strip with 3 μm width, respectively. Two metallic cylinders with a radius of 0.5 μm are embedded in an insulating host, and the total thickness of the strip is 100 nm, which is the same as the actual thickness of the PCSMO film used in our experiments. (e−g) Comparison of line-scanned in-plane and out-of-plane *E*-field intensities at the interface and middle plane of the strip. Each curve is taken along the diametrical direction of the metal cylinder (black line in b, c, and d).

kV/cm decreases largely from 44 to 23% as the strip width decreases from 50 to 20 μm (see Figure 3c,d). Similar reduction of modulation amplitude also appears in the modulation of T_{MI} (from 7.8 to 5.0%; see Figure 3e,f). This large reduction of modulation amplitude indicates that the dominant role of strain effect attenuates over the width narrowing, becoming less active. The increasing strain relaxation due to the strip narrowing should be the main reason for the weakness of strain effect. Moreover, it is noted that ρ_p and T_{MI} of the 50 μm (20 μm) strip exhibits 11 and 15% (2.2 and 0.1%) differences, respectively, for external fields of +4 and −4 kV/cm (see Figure 3c,e). This result suggests that a built-in field may exist and affect the strain-mediated field modulation of transport properties, consistent with the small asymmetry in the butterfly ε−E curve. However, the small value of the difference indicates that the built-in electric field may have little effect on the polarity-independent field modulation behaviors in our samples.

More interestingly, a completely different modulation mode emerges and dominates over the field-modulating behavior at narrow strips. Figure 4 shows the detailed results in narrow strips under various bias *E*-fields. The resistivity (both at respective transition temperature and at fixed temperature) of each narrow strip decreases with the positive gate voltage and increases with the negative one, while the transition temperature T_{MI} does the opposite. This asymmetric modulation for the field with different polarities suggests that the strain effect is trivial in narrower strips. Meanwhile, the opposite modulation for positive and negative gate voltages indicates that a polarity dependence for the field modulation of transport behaviors emerges in the narrow strip. Moreover, it is found that the modulation amplitudes of ρ_p and T_{MI} between the fields of 4 and −4 kV/cm increase about 6 and 2 times (see Figure 5a), respectively, as the strip width reduces from 10 to 3 μm. Accordingly, the modulation ratio (defined as a ratio of the half modulation amplitude to the mean value of ρ_p and T_{MI} under 4 and −4 kV/cm) increases from 45 to 92% for ρ_p and 8.7 to 26% for T_{MI} (Figure 5b). This large enhancement of the modulation amplitude with dimension reduction of the PCSMO channel film should be ascribed to the steep decline of possible percolation paths due to the spatial confinement, which provides the phase-separation material with a special advantage in the practical field modulation device with micro- or nanosize.

DOI: 10.1021/acsami.8b10915
ACS Appl. Mater. Interfaces 2018, 10, 32597−32606

Meanwhile, one may also note that the modulation amplitudes (and ratios) in narrower strips ($\leq$10 μm) are much larger than those in wider strips, indicating that the polarity-dependent field modulation is stronger than the polarity-independent one due to the field-induced strain effect in the system exhibiting phase separation.

Moreover, a voltage/E-field hysteresis in the modulating process appears in these narrow strips and develops with the width reducing (see Figure 4d−l). As a result, after the removal of electric bias field, ρ_p, ρ_T, and T_{MI} gradually approach the one under the field of 4 kV/cm, showing a growing nonvolatile behavior in the polarity-dependent area ($\leq$10 μm). Typically, when the width of the strip narrows down to 3 μm, ρ_p, ρ_T, and T_{MI} keep nearly unchanged after the removal of the bias field. In addition, one could find that the hysteresis width increases on reducing the strip width. Specially, the reversal field for the 3 μm strip is consistent with the coercive field of the PMN−PT substrate (~2 kV/cm). These results indicate that the transport modulation in narrower strips is closely related with the polarization field, regardless of the screening effect at the interface between the PCSMO film and the PMN−PT substrate.

Previous research on manganite−piezoelectric heterostructural films have demonstrated that the polarization field would accumulate charge between separated metallic and semiconducting or insulating phases, resulting in the variation of the relative volume fractions of metallic and semiconducting (or insulating) regions and thus metallicity and T_{MI} of the film.[20] At first glance, one may attribute the observed polarity-dependent transport behavior in narrow strips to such polarization field effect. However, careful examination finds that the direction of the variation in metallicity and T_{MI} arising from the bias field is totally contrary to previously observed polarization field effect where a positive (negative) field depletes (accumulates) the holes in the film and leads to a decrease (increase) of metallicity and T_{MI}.[20,30,33] Since the direction of bias field polarity is identical both in our experiment (see Figure 2b) and in previous reported polarization effect,[20,30,33] one could affirm that a completely opposite polarity-dependency relationship emerges in the present electrostatic field effect. Such anomalous polarity-dependence appearing in narrow strips suggests that the electrostatic modulation in a spatial-confined system may be driven by a new mechanism. Considering that the bias electric field or polarization field on the substrate could penetrate deeply into the electronically inhomogeneous manganite film regardless of screening effect,[20,30,33] it is reasonable to speculate that the distribution of the induced electric field may play a key role in generating the present distinct anomalous field effect in the spatial-confined manganite film.

To further understand this anomalous polarity-dependent field modulation behavior, the electric field distribution in the PCSMO strip was calculated by using a three-dimensional finite-element model (Figure 6a), in which three-dimensional dielectric matrices are constructed with the same geometry as the experimental devices. The size of the substrate cuboid and the length of strips (assigned as 2 times the width of the strip) were chosen to closely align with actual experimental conditions, taking into account requirements from saving computational cost. In the simulation, metallic cylinders with a radius of 0.5 μm are embedded in an insulating host, presenting the inhomogeneous distribution of metallic and COI phases. The metallic and COI phases in PCSMO strips are assigned dielectric constants of 55 000 and 35,[30,50] respectively, while the dielectric values of the PMN−PT substrate and vacuum are set to 5000 and 1, respectively.[51,52] An electric field of 4 kV/cm with both polarity is applied on the substrate, and the electric field in the strip is calculated by solving the differential equation of Gauss' law ($\nabla \cdot D = 0$, where D is the electric displacement field) across the matrices. It is noted that altering the polarity of the applied bias field only results in a change of sign for the calculated E-field intensity. Thus, only results under the bias field with positive polarity whose direction is defined as pointing from bottom to top (see Figures 2b and 6a) are presented.

Figure 6b−d shows the distribution of in-plane (E_x, E_y) and out-of-plane (E_z) E-field intensities in the interface plane between the film and substrate for the selected strip with 3 μm width. Two key findings from the simulated results are that the induced polarization field in the strip has a large in-plane component and shows a highly localized state around the metallic edge. Figure 6e−g presents the comparison of line-scanned in-plane and out-of-plane E-field intensities at the interface and middle plane parallel to the surface, respectively. It is seen that the in-plane field exhibits a maximum value (~790 kV/cm) at the interface between the COI and FMM phases and decays in the COI region. In addition, the results in Figure 6 demonstrate that the direction of the in-plane polarization field points from the surrounding COI phase toward the center FMM one. Moreover, the induced polarization/electric field decays slowly with an almost linear feature along the thickness direction, suggesting that the induced field not only locates near the interface but also penetrates deeply into the channel film. Typically, a maximum value of ~350 kV/cm (nearly half of the one at the interface plane) is induced in the middle plane (see Figure 6e,f). This result demonstrates that the modulating effect by the induced in-plane field is not limited to interfacial layers adjacent to the substrate. Besides, it is found that the absolute value of the induced in-plane polarization field varies a little around the edge of metal cylinders, which should be attributed to the edge effect originating from the discontinuous medium boundary condition (see Section I of the Supporting Information for a more detailed discussion).

It is noted that the electric field (or polarization field) induced in the strip has an out-of-plane component (see Figure 6d,g), which also increases with the reduction of the strip width. Recent reports on real-space domain observations using a microwave impedance microscope demonstrate that the typical domain size in $Pr_{0.55}(Ca_{0.75}Sr_{0.25})_{0.45}MnO_3$ thin films is 500 nm to 1 μm,[53,54] which is much larger than the thickness of our strips. As a result, the creation of a domain wall (between metallic and insulating phases) parallel to the surface in the present strips would cost too much domain wall energy.[54] Therefore, the role of the induced out-of-plane polarization field should be trivial in observed polarity-dependent modulation behaviors. Instead, the large in-plane polarization field, which could drive a phase transition near the edge of FMM domains, may be the main cause of the anomalous polarity-dependent field effect observed in the present narrow PCSMO strips. Moreover, calculated results show that the in-plane polarization field could appear, induced by an external bias, near the metal region in all experimental strips. Meanwhile, the maximum value of the induced in-plane field increases quickly from 450 to 790 kV/cm when the strip width decreases from 10 to 3 μm, indicating the great facilitation from spatial confinement.

Furthermore, many experimental and theoretical investigations have previously shown that FM tendencies could appear in the nanosized antiferromagnetic CO manganites due to the inhomogeneous charge distribution at the surface.[55−58]

DOI: 10.1021/acsami.8b10915
ACS Appl. Mater. Interfaces 2018, 10, 32597−32606

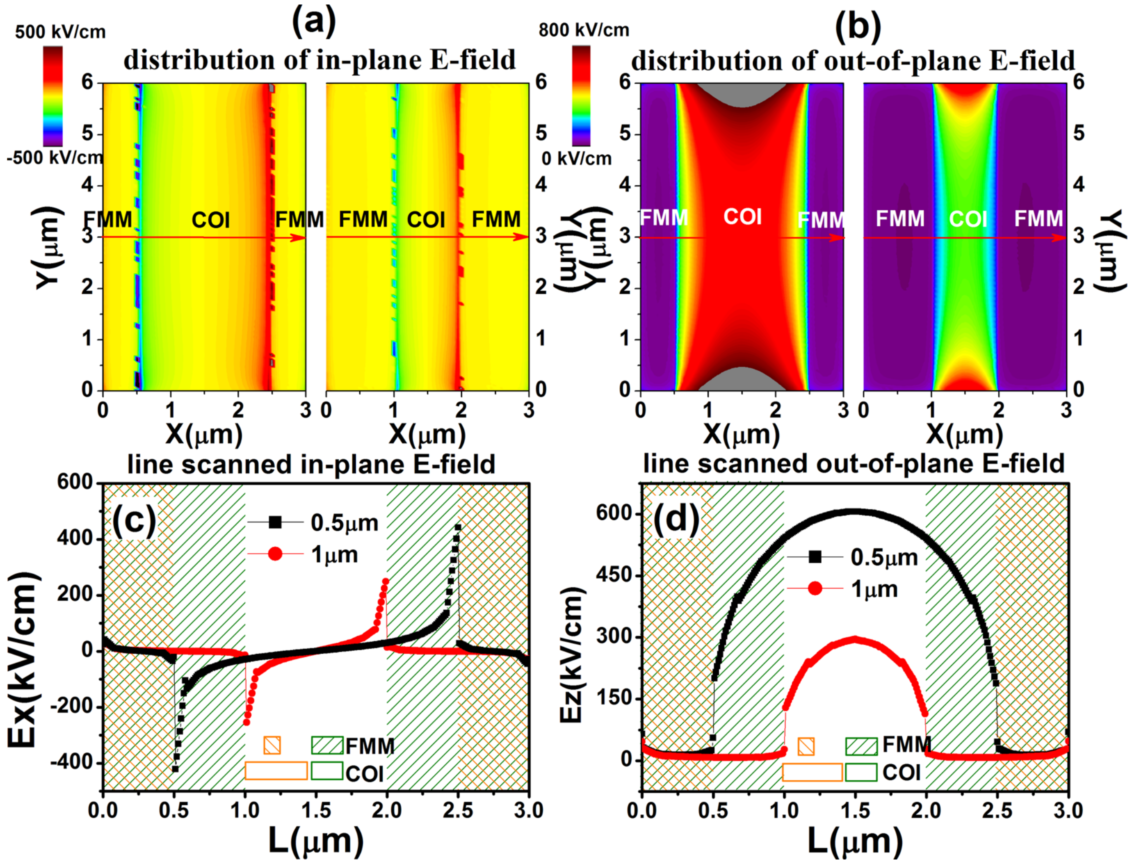

Figure 7. Two-dimensional distribution of (a) in-plane and (b) out-of-plane E-field intensities in the interface plane under +4 kV/cm bias field for the 3 μm strip with symmetric FMM edge state in each side, whose width is set to 0.5 and 1 μm, respectively. Comparison of (c) line-scanned in-plane and (d) out-of-plane E-field intensities for strips with different-width FMM edge state. Each curve is taken along the red line in (a) and (b), respectively.

Recently, Shen et al. further observed a clear FMM phase with a width of ~1 μm at the edge side of spatial-confined PS strips, which was attributed to the broken symmetry effect.[38] It is reasonable to believe that a similar FMM edge state also appears, in our experiments, considering similar phase separation behaviors and an abnormal increase of metallicity and T_{MI} in the narrow PCSMO strip (see Figure 2c). Obviously, the induced in-plane polarization field in the strip should also be affected by the appearance of the FMM edge state. Taking into account the existence of the FMM edge phase, the distribution of the electric field is further calculated with dielectric values of 55 000 and 35 assigned to FMM edge phases and COI phases.[30,51] According to the reported characteristics of the FMM edge state and real configuration of strips in our experiments, we set the FMM edge state area as a long narrow cuboid along the y-direction. Moreover, considering that the FMM−COI interface is parallel to E_y, the role of in-plane E_y is presumed to be trivial in the strip with FMM edge state (see Section II of the Supporting Information for a more detailed discussion). Figure 7 shows the two-dimensional distribution and line scan of E-field intensity for the 3 μm strip with symmetric 0.5 and 1 μm-wide FMM edge phases at both sides. It is seen that a large in-plane electric field (~420 kV/cm for the strip with 0.5 μm-wide FMM edge phase and ~250 kV/cm for the 1 μm-wide one) appears at the interface between the FMM edge phase and the central COI phase and extends to the center of the strip (the COI or phase coexistence regions) with an attenuated intensity. Meanwhile, a negligible in-plane E-field is identified in edge regions, which should be attributed to the screening effect from the metal characteristic of the FMM edge phase. It is worthy to point out that the E-field intensity calculated in the strip with cylinder-shaped metal area is almost twice as large as the one in the strip with cuboid FMM edge area (see Figures 6e−g and 7c−d), demonstrating the enhancement of E-field in the area with large curvature. This result indicates that the induced electric/polarization field in the phase-separated region can be largely affected by the shape of coexisting phases.

These large local in-plane electric/polarization fields shown in Figures 6 and 7 would induce a local phase transition near the FMM−COI interface and move the interface by accumulating charges between the FMM edge phase and the COI phase[20,23,30,52] and thus change the relative volume fraction of metallic and insulating regions. The nature of accumulated charges, electrons or holes, depending on the polarity of the induced in-plane electric field, controls the direction of interface movement. In our case, applying a positive bias E-field on the FE substrate (which points from bottom to top) induces an in-plane polarization field in the strip, with the direction pointing from the COI phase to the FMM phase (see Figures 6a,e,f and 7c). Such in-plane field would cause an accumulation of holes in the interface between FMM and COI phases and push the interface to the COI region, leading to the rebuilding of percolation channel and thus increased metallicity and T_{MI} in the strip. A negative bias E-field on the substrate does the opposite, leading to a decrease in the metallicity and T_{MI}. Obviously, the modulating direction under this new mechanism is completely opposite to the one in normal polarization effect, where a

DOI: 10.1021/acsami.8b10915
ACS Appl. Mater. Interfaces 2018, 10, 32597−32606

positive bias results in a decreased metallicity and T_{MI}. More interestingly, it is found that the lateral *E*-field (or induced in-plane polarization field) at the interface (between the FMM edge phase and the central COI phase) decreases with the width of the FMM edge state (see Figure 7c), indicating that the expansion of the FMM edge state, driven by the interface polarization field, may be a negative feedback process. Moreover, the stronger modulation behavior in the 3 μm-sample indicates that the FMM edge state could be largely altered by electrical bias, providing a new channel to understand the edge state in spatial-confined complex oxides and its underlying principle.

This picture gives a good qualitative match to experimental observations of enhanced modulation amplitude and anomalous polarity-dependence of the field modulation in narrow PCSMO strips. Actually, simulated results show that the intensity of the in-plane electric field increases with the reduction of the strip width, indicating the enhancement of the anomalous field effect at narrow strips. Moreover, the limited percolation channel in narrower strips further enhances the modulation sensitivity, resulting in an enhanced modulation amplitude around the percolation transition temperature in narrow strips. Besides, in the narrow strip with FMM edge state, the large FMM−COI interface area also increases the tuning sensitivity, leading to a largely enhanced modulation behavior. Meanwhile, instead of the polarity-independent strain effect, the anomalous polarity-dependent field effect becomes the dominant factor in driving field modulation as the strip narrows down. Accordingly, a transition from polarity independence to anomalous polarity-dependence emerges in field modulation behaviors (see Figures 3 and 4). Moreover, the experimentally observed nonvolatile modulation of transport behaviors is also naturally explained within this framework. As is well known, the phase transition driven by the induced in-plane polarization field in narrow strips has a first-order nature, possessing a definite hysteresis. As a result, the modulation due to the phase transition remains unchanged after the removal of the bias field, providing the nonvolatility of the electrostatic field effect in the narrow strip.

IV. CONCLUSIONS

In summary, a greatly enhanced modulation amplitude and anomalous polarity-dependence, facilitated by dimension reduction, are discovered in an oxide-based FET prototype device with a spatial-confined $Pr_{0.7}(Ca_{0.6}Sr_{0.4})_{0.3}MnO_3$ channel film. Our studies demonstrate that lateral configurations of electronic phase separation and thus the percolation channel, in structures confined to length scales similar to that of the phase domains, can be nonvolatile modified by a small vertical electric field through the induced in-plane polarization field, showing a new acting channel of geometric control of nanoscale electronic phase separation and macroscopic transport behaviors. This special acting mechanism and underlying experimental phenomena offer new possibilities for designing high-effective and easy-implemented all-oxide-based electronic devices, such as low-power field-effect switching and nonvolatile memory devices. Further development of the phenomena may bring new types of multifunctionality to other strongly correlated materials where electronic phase competition exists.

■ ASSOCIATED CONTENT

Supporting Information

The Supporting Information is available free of charge on the ACS Publications website at DOI: 10.1021/acsami.8b10915.

In-plane *E*-field variation around the edge of metal cylinders and the influence of E_y on the FMM−COI interface variation for the 3 μm strip with FMM edge state (PDF)

■ AUTHOR INFORMATION

Corresponding Authors

*E-mail: wangjing@iphy.ac.cn (J.W).
*E-mail: fxhu@iphy.ac.cn (F.H.).

ORCID

Jing Wang: 0000-0001-5458-6711
Jirong Sun: 0000-0003-1238-8770

Notes

The authors declare no competing financial interest.

■ ACKNOWLEDGMENTS

This work was supported by the National Key Research and Development Program of China (Grant Nos 2017YFA0303601, 2017YFB0702702, and 2016YFA0300701), the National Natural Sciences Foundation of China (Grant Nos 11474341, 11674378, 51531008, 51590880, and 51771223), and the Key Program of the Chinese Academy of Sciences and the Strategic Priority Research Program (B) of the Chinese Academy of Sciences.

■ REFERENCES

(1) Shenoy, V. B.; Sarma, D. D.; Rao, C. N. R. Electronic Phase Separation in Correlated Oxides: The Phenomenon, Its Present Status and Future Prospects. *ChemPhysChem* **2006**, *7*, 2053−2059.

(2) Sharoni, A.; Ramírez, J. G.; Schuller, I. K. Multiple Avalanches across the Metal-Insulator Transition of Vanadium Oxide Nanoscaled Junctions. *Phys. Rev. Lett.* **2008**, *101*, No. 026404.

(3) Basov, D. N.; Averitt, R. D.; Van der Marel, D.; Dressel, M.; Haule, K. Electrodynamics of Correlated Electron Materials. *Rev. Mod. Phys.* **2011**, *83*, 471−541.

(4) Mathur, N. D.; Littlewood, P. B. The Self-Organised Phases of Manganites. *Solid State Commun.* **2001**, *119*, 271−280.

(5) Tokura, Y. *Colossal Magnetoresistive Oxides*; Gordon and Breach Science Publishers, 2000.

(6) Mathews, S.; Ramesh, R.; Vankatesan, T.; Benedetto, J. Ferroelectric Field Effect Transistor Based on Epitaxial Perovskite Heterostructures. *Science* **1997**, *276*, 238−240.

(7) Tanaka, H.; Zhang, J.; Kawai, T. Giant Electric Field Modulation of Double Exchange Ferromagnetism at Room Temperature in the Perovskite Manganite/Titanate p-n Junction. *Phys. Rev. Lett.* **2002**, *88*, No. 027204.

(8) Ahn, C. H.; Bhattacharya, A.; Di Ventra, M.; Eckstein, J. N.; Frisbie, C. D.; Gershenson, M. E.; Goldman, A. M.; Inoue, I. H.; Mannhart, J.; Millis, A. J.; Morpurgo, A. F.; Natelson, D.; Triscone, J. M. Electrostatic Modification of Novel Materials. *Rev. Mod. Phys.* **2006**, *78*, 1185−1212.

(9) Ohno, H.; Chiba, D.; Matsukura, F.; Omiya, T.; Abe, E.; Dietl, T.; Ohno, Y.; Ohtani, K. Electric-Field Control of Ferromagnetism. *Nature* **2000**, *408*, 944−946.

(10) Yamada, Y.; Ueno, K.; Fukumura, T.; Yuan, H. T.; Shimotani, H.; Iwasa, Y.; Gu, L.; Tsukimoto, S.; Ikuhara, Y.; Kawasaki, M. Electrically Induced Ferromagnetism at Room Temperature in Cobalt-Doped Titanium Dioxide. *Science* **2011**, *332*, 1065−1067.

(11) Caviglia, A. D.; Gariglio, S.; Reyren, N.; Jaccard, D.; Schneider, T.; Gabay, M.; Thiel, S.; Hammerl, G.; Mannhart, J.; Triscone, J. -M Electric Field Control of the $LaAlO_3/SrTiO_3$ Interface Ground State. *Nature* **2008**, *456*, 624−627.

(12) Ueno, K.; Nakamura, S.; Shimotani, H.; Ohtomo, A.; Kimura, N.; Nojima, T.; Aoki, H.; Iwasa, Y.; Kawasaki, M. Electric-Field-Induced Superconductivity in an Insulator. *Nat. Mater.* **2008**, *7*, 855−858.

(13) Bollinger, A. T.; Dubuis, G.; Yoon, J.; Pavuna, D.; Misewich, J.; Bozovic, I. Superconductor-Insulator Transition in $La_{2-x}Sr_xCuO_4$ at the Pair Quantum Resistance. *Nature* **2011**, *472*, 458−460.
(14) Hong, X.; Posadas, A.; Lin, A.; Ahn, C. H. Ferroelectric-Field-Induced Tuning of Magnetism in the Colossal Magnetoresistive Oxide $La_{1-x}Sr_xMnO_3$. *Phys. Rev. B* **2003**, *68*, No. 134415.
(15) Scherwitzl, R.; Zubko, P.; Lezama, I. G.; Ono, S.; Morpurgo, A. F.; Catalan, G.; Triscone, J.-M. Electric-Field Control of the Metal-Insulator Transition in Ultrathin NdNiO3 Films. *Adv. Mater.* **2010**, *22*, 5517−5520.
(16) Tokura, Y. Correlated-Electron Physics in Transition-Metal Oxides. *Phys. Today* **2003**, *56*, 50−55.
(17) Ahn, C. H.; Triscone, J.-M.; Mannhart, J. Electric Field effect in Correlated Oxide Systems. *Nature* **2003**, *424*, 1015−1018.
(18) Inoue, I. H. Electrostatic Carrier Doping to Perovskite Transition-Metal Oxides. *Semicond. Sci. Technol.* **2005**, *20*, S112−S120.
(19) Chakhalian, J.; Millis, A. J.; Rondinelli, J. Whither the Oxide Interface. *Nat. Mater.* **2012**, *11*, 92−94.
(20) Wu, T.; Ogale, S. B.; Garrison, J. E.; Nagaraj, B.; Biswas, A.; Chen, Z.; Greene, R. L.; Ramesh, R.; Venkatesan, T.; Millis, A. J. Electroresistance and Electronic Phase Separation in Mixed-valent Manganites. *Phys. Rev. Lett.* **2001**, *86*, 5998−6001.
(21) Ogale, S. B.; Talyansky, V.; Chen, C. H.; Ramesh, R.; Greene, R. L.; Venkatesan, T. Unusual Electric Field effects in $Nd_{0.7}Sr_{0.3}MnO_3$. *Phys. Rev. Lett.* **1996**, *77*, 1159−1162.
(22) Pallecchi, I.; Pellegrino, L.; Bellingeri, E.; Siri, A. S.; Marré, D. Effects of Electric and Magnetic Fields on Phase-Separated $La_{0.7}Sr_{0.3}MnO_3$-delta Thin Films. *Phys. Rev. B* **2005**, *71*, No. 014406.
(23) Hong, X.; Posadas, A.; Ahn, C. H. Examining the Screening Limit of Field Effect Devices via the Metal-Insulator Transition. *Appl. Phys. Lett.* **2005**, *86*, No. 142501.
(24) Thiele, C.; Dörr, K.; Schultz, L.; Beyreuther, E.; Lin, W. M. Piezoelectrically Induced Resistance Modulations in $La_{0.7}Sr_{0.3}MnO_3$/$Pb(Zr,Ti)O_3$ Field Effect Devices. *Appl. Phys. Lett.* **2005**, *87*, No. 162512.
(25) Zheng, R. K.; Wang, Y.; W. Chan, H. L.; Choy, C. L.; Luo, H. S. Strain-Mediated Electric-Field Control of Resistance in the $La_{0.85}Sr_{0.15}MnO_3$/0.7$Pb(Mg_{1/3}Nb_{2/3})O_3$-0.3$PbTiO_3$ Structure. *Appl. Phys. Lett.* **2007**, *90*, No. 152904.
(26) Zhao, Y. Y.; Wang, J.; Kuang, H.; Hu, F. X.; Zhang, H. R.; Liu, Y.; Zhang, Y.; Wang, S. H.; Wu, R. R.; Zhang, M.; Bao, L. F.; Sun, J. R.; Shen, B. G. Abnormal Percolative Transport and Colossal Electro-resistance Induced by Anisotropic Strain in (011)-$Pr_{0.7}(Ca_{0.6}Sr_{0.4})_{0.3}MnO_3$/PMN-PT heterostructure. *Sci. Rep.* **2014**, *4*, No. 7075.
(27) Wu, T.; Bur, A.; Wong, K.; Zhao, P.; Lynch, C. S.; Amiri, P. K.; Wang, K. L.; Carman, G. P. Electrical Control of Reversible and Permanent Magnetization Reorientation for Magnetoelectric Memory Devices. *Appl. Phys. Lett.* **2011**, *98*, No. 262504.
(28) Wu, T.; Bur, A.; Zhao, P.; Mohanchandra, K. P.; Wong, K.; Wang, K. L.; Lynch, C. S.; Carman, G. P. Giant Electric-Field-Induced Reversible and Permanent Magnetization Reorientation on Magnetoelectric Ni/(011) $[Pb(Mg_{1/3}Nb_{2/3})O_3]_{1-x}[PbTiO_3]_x$ heterostructure. *Appl. Phys. Lett.* **2011**, *98*, No. 012504.
(29) Yang, Y. J.; Luo, Z. L.; Yang, M. M.; Huang, H. L.; Wang, H. B.; Bao, J.; Pan, G. Q.; Gao, C.; Hao, Q.; Wang, S. T.; Jokubaitis, M.; Zhang, W. Z.; Xiao, G.; Yao, Y. P.; Liu, Y. K.; Li, X. G. Piezo-strain induced non-volatile resistance states in (011)-$La_{2/3}Sr_{1/3}MnO_3$/0.7$Pb(Mg_{2/3}Nb_{1/3})O_3$-0.3$PbTiO_3$ epitaxial heterostructures. *Appl. Phys. Lett.* **2013**, *102*, No. 033501.
(30) Lourembam, J.; Wu, J. C.; Ding, J. F.; Lin, W. N.; Wu, T. Electric Field Tuning of Phase Separation in Manganite Thin Films. *Phys. Rev. B* **2014**, *89*, No. 014425.
(31) Thiele, C.; Dörr, K.; Bilani, O.; Rödel, J.; Schultz, L. Influence of Strain on the Magnetization and Magnetoelectric Effect in $La_{0.3}A_{0.7}MnO_3$/PMN-PT(001) (A = Sr,Ca). *Phys. Rev. B* **2007**, *75*, No. 054408.
(32) Sheng, Z. G.; Gao, J.; Sun, Y. P. Coaction of Electric Field Induced Strain and Polarization Effects in $La_{0.7}Ca_{0.3}MnO_3$/PMN-PT structures. *Phys. Rev. B* **2009**, *79*, No. 174437.
(33) Jiang, T.; Yang, S. W.; Liu, Y. K.; Yin, Y. W.; Dong, S. N.; Zhao, W. B.; Li, X. G. Coaction and distinguishment of converse piezoelectric and field effects in $La_{0.7}Ca_{0.3}MnO_3$/$SrTiO_3$/0.68$Pb(Mg_{1/3}Nb_{2/3})O_3$-0.32$PbTiO_3$ heterostructures. *Appl. Phys. Lett.* **2013**, *103*, No. 053504.
(34) Guo, H.; Noh, J. H.; Dong, S.; Rack, P. D.; Gai, Z.; Xu, X. S.; Dagotto, E.; Shen, J.; Ward, T. Z. Electrophoretic-like Gating Used To Control Metal-Insulator Transitions in Electronically Phase Separated Manganite Wires. *Nano Lett.* **2013**, *13*, 3749−3754.
(35) Singh-Bhalla, G.; Selcuk, S.; Dhakal, T.; Biswas, A.; Hebard, A. F. Intrinsic Tunneling in Phase Separated Manganites. *Phys. Rev. Lett.* **2009**, *102*, No. 077205.
(36) Nakajima, T.; Tsuchiya, T.; Ueda, Y.; Kumagai, T. Probing Electronic-Phase-Separated Insulating Domains In the Metallic Phase of Patterned Perovskite Manganite Microwires. *Phys. Rev. B* **2009**, *80*, No. 020401(R).
(37) Ward, T. Z.; Liang, S.; Fuchigami, K.; Yin, L. F.; Dagotto, E.; Plummer, E. W.; Shen, J. Reemergent Metal-Insulator Transitions in Manganites Exposed with Spatial Confinement. *Phys. Rev. Lett.* **2008**, *100*, No. 247204.
(38) Du, K.; Zhang, K.; Dong, S.; Wei, W. G.; Shao, J.; Niu, J. B.; Chen, J. J.; Zhu, Y. Y.; Lin, H. X.; Yin, X. L.; Liou, S. H.; Yin, L. F.; Shen, J. Visualization of a Ferromagnetic Metallic Edge State in Manganite Strips. *Nat. Commun.* **2015**, *6*, No. 6179.
(39) Ward, T. Z.; Zhang, X. G.; Yin, L. F.; Zhang, X. Q.; Liu, M.; Snijders, P. C.; Jesse, S.; Plummer, E. W.; Cheng, Z. H.; Dagotto, E.; Shen, J. Time-Resolved Electronic Phase Transitions in Manganites. *Phys. Rev. Lett.* **2009**, *102*, No. 087201.
(40) Marín, L.; Morellón, L.; Algarabel, P. A.; Rodríguez, L. A.; Magén, C.; De Teresa, J. M.; Ibarra, M. R. Enhanced Magnetotransport in Nanopatterned Manganite Nanowires. *Nano Lett.* **2014**, *14*, 423−428.
(41) Zhai, H.-Y.; Ma, J. X.; Gillaspie, D. T.; Zhang, X. G.; Ward, T. Z.; Plummer, E. W.; Shen, J. Giant Discrete Steps in Metal-Insulator Transition in Perovskite Manganite Wires. *Phys. Rev. Lett.* **2006**, *97*, No. 167201.
(42) Tomioka, Y.; Tokura, Y. Bicritical Features of the Metal-Insulator Transition in Bandwidth-Controlled Manganites: Single Crystals of $Pr_{1-x}(Ca_{1-y}Sr_y)_xMnO_3$. *Phys. Rev. B* **2002**, *66*, No. 104416.
(43) Sharma, P. A.; Kim, S. B.; Koo, T. Y.; Guha, S.; Cheong, S.-W. Reentrant Charge Ordering Transition in the Manganites as Experimental Evidence for a Strain Glass. *Phys. Rev. B* **2005**, *71*, No. 224416.
(44) Dhakal, T.; Tosado, J.; Biswas, A. Effect of Strain and Electric Field on the Electronic Soft Matter in Manganite Thin Films. *Phys. Rev. B* **2007**, *75*, No. 92404.
(45) Milward, G. C.; Calderon, M. J.; Littlewood, P. B. Electronically Soft Phases in Manganites. *Nature* **2005**, *433*, 607−610.
(46) Zhang, L.; Israel, C.; Biswas, A.; Greene, R. L.; de Lozanne, A. Direct Observation of Percolation in a Manganite Thin Film. *Science* **2002**, *298*, 805−807.
(47) Ghivelder, L.; Parisi, F. Dynamic Phase Separation in $La_{5/8-y}Pr_yCa_{3/8}MnO_3$. *Phys. Rev. B* **2005**, *71*, No. 184425.
(48) Wu, T.; Mitchell, J. F. Creation and Annihilation of Conducting Filaments in Mesoscopic Manganite Structures. *Phys. Rev. B* **2006**, *74*, No. 214423.
(49) Biegalski, M. D.; Dörr, K.; Kim, D. H.; Christen, H. M. Applying Uniform Reversible Strain to Epitaxial Oxide Films. *Appl. Phys. Lett.* **2010**, *96*, No. 151905.
(50) Kundys, B.; Bellido, N.; Martin, C.; Simon, C. Dielectric Catastrophe at the Magnetic Field Induced Insulator to Metal Transition in $Pr_{1-x}Ca_xMnO_3$(x = 0.30, 0.37) Crystals. *Eur. Phys. J. B* **2006**, *52*, 199.
(51) Sun, E.; Cao, W. W. Relaxor-Based Ferroelectric Single Crystals: Growth, Domain Engineering, Characterization and Applications. *Prog. Mater. Sci.* **2014**, *65*, 124−210.

(52) Dong, S.; Zhu, C.; Wang, Y.; Yuan, F.; Wang, K. F.; Liu, J.-M. Electric Field Induced Collapse of the Charge-Ordered Phase in Manganites. *J. Phys.: Condens. Matter* **2007**, *19*, No. 266202.

(53) Kundhikanjana, W.; Sheng, Z. G.; Yang, Y.; Lai, K. J.; Ma, E. Y.; Cui, Y. T.; Kelly, M. A.; Nakamura, M.; Kawasaki, M.; Tokura, Y.; Tang, Q. C.; Zhang, K.; Li, X. X.; Shen, Z. X. Direct Imaging of Dynamic Glassy Behavior in a Strained Manganite Film. *Phys. Rev. Lett.* **2015**, *115*, No. 265701.

(54) Hatano, T.; Sheng, Z. G.; Nakamura, M.; Nakano, M.; Kawasaki, M.; Iwasa, Y.; Tokura, Y. Gate Control of Percolative Conduction in Strongly Correlated Manganite Films. *Adv. Mater.* **2014**, *26*, 2874−2877.

(55) Rao, S. S.; Tripathi, S.; Pandey, D.; Bhat, S. V. Suppression of Charge Order, Disappearance of Antiferromagnetism, and Emergence of Ferromagnetism in $Nd_{0.5}Ca_{0.5}MnO_3$ Nanoparticles. *Phys. Rev. B* **2006**, *74*, No. 144416.

(56) Sarkar, T.; Ghosh, B.; Raychaudhuri, A. K.; Chatterji, T. Crystal Structure and Physical Properties of Half-Doped Manganite Nanocrystals of Less Than 100-nm Size. *Phys. Rev. B* **2008**, *77*, No. 235112.

(57) Biswas, A.; Samanta, T.; Banerjee, S.; Das, I. Influence of Charge Ordering on Magnetocaloric Properties of Nanocrystalline $Pr_{0.65}(Ca_{0.7}Sr_{0.3})_{0.35}MnO_3$. *Appl. Phys. Lett.* **2008**, *92*, No. 212502.

(58) Dong, S.; Yu, R.; Yunoki, S.; Liu, J.-M.; Dagotto, E. Ferromagnetic Tendency at the Durface of CE-type Charge-Ordered Manganites. *Phys. Rev. B* **2008**, *78*, No. 064414.

DOI: 10.1021/acsami.8b10915
ACS Appl. Mater. Interfaces 2018, 10, 32597−32606